# Detection of Oil Spills by Remote Sensing Techniques: Comparison of the Use of Radar Images and Optical Images

**Beatriz Mendes**[1],

[1] NOVA University of Lisbon – NOVA IMS, Tel.: +351 926 074 551; 20230919@novaims.unl.pt

Postgraduate in Geospatial Data Science - Remote Sensing

**Abstract**: Oil spills are accidents that harm the marine environment in various parts of the world, potentially contaminating large bodies of water or even coral reefs. Thus, the identification and monitoring of oil spills become very important for biodiversity protection to reduce the environmental and economic problems generated by these accidents. This study aims to discuss and compare the detection of oil spills using radar (SAR) and optical images from the Sentinel-1 and Sentinel-2 satellites, respectively. For this analysis, the oil spill in August 2020 in Mahébourg on the island of Mauritius was defined as the study object. Firstly, the technical specifications of the maps to be produced were established, and subsequently, satellite images were selected for the initial phase and the phase of higher intensity of the accident. After collecting the images, the first steps were the exploratory analysis to understand the characteristics of the images, the definition of the cartographic production strategy, and geographic stratification. Then, image pre-processing and band transformation were carried out. In the case of radar (SAR) images, the ESRI "oil spill detection" Deep Learning model was used to identify the presence of oil. For optical images, a supervised classification was performed in four classes (land, water, oil, and sediments), applying the “Oil Spill Index (OSI): ((B03+B04) / B02)” and band composition "R: (5+6)/7; G: (3+4)/2 B: (11+12)/8". Finally, the accuracy of the models was evaluated by comparing the results with confirmed incident reports and verifying the differences between radar and optical image observations.

**Keywords**: Remote sensing, oil detection, supervised classification, Deep Learning, SAR, optical, Sentinel-1, Sentinel-2.

## 1. Introduction

Oil production plays a very important role in the world economy, with approximately 30% of oil production taking place at sea, and about 60% of all produced oil being transported by sea (IAE 2013). After the stranding of a ship carrying oil or its derivatives, there is a high probability of an oil spill, which is very harmful to the environment and can even have an irreversible impact. Therefore, the study of these events becomes relevant as, through data obtained from active and passive satellite sensors, it is possible to monitor, detect, and map oil spills (Rajendran et al. 2021). Thus, the main objectives of this study are to detect oil slicks resulting from a spill that occurred in August 2020 southeast of the island of Mauritius using Synthetic Aperture Radar (SAR) and multispectral optical images and to compare the results of both.

## 2. Study Area

The oil spill from the Japanese-origin ship MV Wakashio, which was carrying fuel oil and diesel, began on August 6, 2020, off the southeast coast of the island of Mauritius near Pointe d'Esny (latitude: 20°10' S and longitude: 57°30' E). The incident occurred in a location approximately 20 meters deep in an area protected by the Ramsar

Convention on Wetlands, an international treaty aimed at the sustainable conservation of wetlands (Rajendran et al. 2021). The study area consists of Blue Bay (Figure 1) and coastal areas with various beaches, channels, and shallow areas with various sediments.

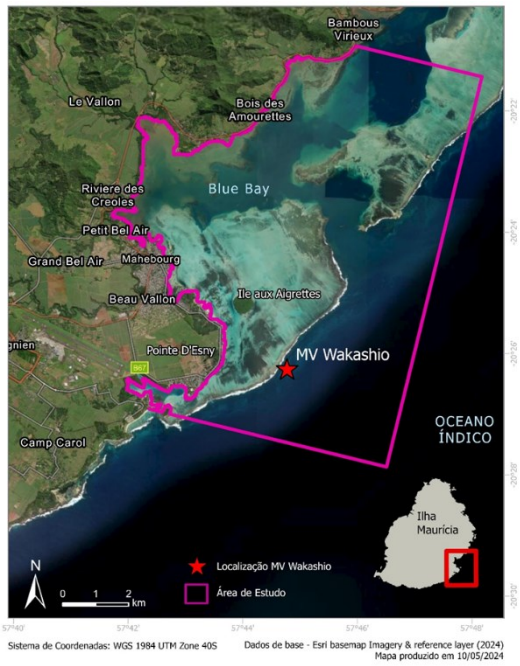


**Figure 1**. Study area

# 3. Satellite Images and Information Extraction Methods

In this study, radar (SAR) images from the polar orbiting Sentinel-1 satellite with a temporal resolution of 12 days and a spatial resolution of 9, 12, and 50 meters were classified. To extract information from the images, the "Oil Spill Detection (SAR)" deep learning model, which is specifically designed and optimized to work with SAR images and allows the identification of oil spills, was used. The model is based on convolutional neural networks (CNNs) which are effective in detecting complex patterns in visual data. In ArcGIS Pro, the model can be applied directly to an input raster through image analysis tools as part of the deep learning workflow available in the software (ESRI 2022; ESRI 2023). The model analyzes the pixels of the SAR image and classifies each pixel based on the probability of being part of an oil spill. This process involves evaluating the texture, contrast, and other spectral characteristics of the pixels. The result is a probability map that highlights areas where there is a high probability of oil spills. The documentation indicates that this model was pre-trained with 381 Sentinel-1 images and has an accuracy of 0.69 (ESRI 2022; ESRI 2023).

Optical images are from the Sentinel-2 satellite, which has a temporal resolution of 10 days, a spatial resolution of 10, 20, and 60 meters, and a spectral resolution ranging from 0.43 to 2.32 µm. It has bands in the visible and infrared spectrum that are useful for this purpose, and in this sense, the following bands were used for image construction (Caetano 2018):

- Visible Bands (B2, B3, B4): These bands capture blue, green, and red light. The blue band (B2) is particularly useful in marine applications for penetrating the water column and detecting sediments and organic matter.
- Near-Infrared Band (B8): This band is effective in detecting surface variations in the water and can help identify surface films such as oil.
- Short-Wave Infrared Bands (11, 12): These bands help identify suspended sediments in the water and highlight chemical variations in the water, including the presence of pollutants or changes in chemical composition.

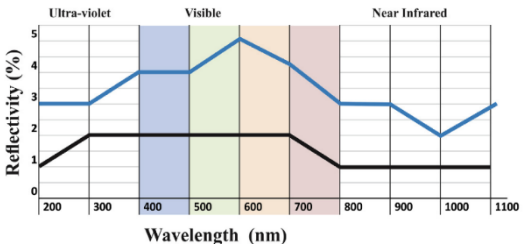


**Figure 2**. Oil (blue) and water (black) Reflectance Lines (Fingas et al., 2014).

As presented in Figure 2, the spectral differences between oil and water are not very pronounced, but the band transformations presented in this report aim to accentuate the distinguishing features and create combinations that allow for positive identification of oil.

To extract information from these images, several steps were necessary, which are described in detail throughout the work, such as:

- Exploratory image analysis
- Pre-processing
- Band transformation
- Segmentation
- Variable selection and classification
- Post-processing
- Supervised automatic classification based on the maximum likelihood classifier considers that the bands have a normal distribution for each sample. With this assumption, the statistical parameters of mean and covariance are calculated for each sample. With these parameters, it is possible to calculate the probability that a given spatial analysis unit belongs to each of the classes defined in the training phase (Caetano 2018). Subsequently, the samples can be evaluated from dendrograms to verify their differences.
- Thematic evaluation serves to assess the accuracy of the results using reference data from oil spills and comparing it with the model used for both SAR and optical images to create confusion matrices. Confusion matrices are a statistical tool that allows evaluating the performance of classification models through the following parameters:
  1. UA (User's Accuracy): Indicates how accurately the model classifies a category as true, i.e., the percentage of positive predictions that were correct. Calculated using the formula:

$$UA = \frac{True\ Positives\ of\ the\ Prediction\ Class}{Total\ Classifications\ of\ the\ Prediction\ Class}$$

  2. PA (Producer's Accuracy): Reflects how well the model managed to identify all real instances of a category, i.e., the percentage of real cases identified correctly. Calculated using the formula

$$PA = \frac{True\ Positives\ of\ the\ Reference\ Class}{Total\ Classifications\ of\ the\ Reference\ Class}$$

  3. OA (Overall Accuracy): The overall accuracy of the model across all categories. Calculated using the formula:

$$OA = \frac{True\ Positives\ and\ Negatives\ Classified}{Total\ Classifications}$$

# 4. Results and Discussion

This chapter addresses two methodologies for extracting information from satellite images at different time points: the phase before the oil spill, the initial phase, and the peak intensity phase of the spill. The first approach uses Sentinel-1 (SAR) images, and deep learning methods classify the areas that should represent the oil slick. The second approach uses Sentinel-2 (multispectral optical) images and a supervised classification to extract areas corresponding to potential oil slicks. The automatic classification methodologies are complemented with visual interpretation of the images.

## 4.1. Preliminary Stages

### 4.1.1. Definition of Technical Specifications of the Maps to be Produced

This project aims to produce thematic cartography from satellite images to detect and delimit oil slicks in oceans. Map production will be done through automatic image classification and validated by computer-assisted visual interpretation. The implemented nomenclature facilitates the interpretation and communication of the data represented in the different stages of analysis, as well as in the production of the final map (Figure 28, Appendix 1). Unlike land use/land cover mapping, which has a

well-defined reference nomenclature, there is no standard for detecting oil spills in oceans. Thus, consulting various bibliographic sources, four different elements were defined for classification: Land, Water, Oil, and Sediments (Table 1). The main element is the vector polygon that will define the probable oil slicks.

**Table 1**. Nomenclature used

| Value | Element |
|---|---|
| 1 | Land |
| 2 | Water |
| 3 | Oil |
| 4 | Sediments |

Environmental legislation and oil spill response protocols vary between countries. In general, environmental agencies establish guidelines for identifying and responding to oil spills based on their size and potential environmental impact. In this analysis, the minimum area for oil slicks was defined as 250 m². This value corresponds to the minimum cartographic unit (MCU), representing the smallest area represented on the map (Caetano 2018).

### 4.1.2. Selection and Acquisition of Satellite Images

As described earlier, this project uses Synthetic Aperture Radar (SAR) - Sentinel-1 and multispectral optical - Sentinel-2 images. Different studies have demonstrated the advantages of using active and passive sensors in detecting oil slicks (Rajendran et al. 2021). The selection of satellites and sensors was based on the availability of images acquired for the appropriate time interval of the incident (before and during the spill), sufficient spatial resolution to detect the elements under analysis, and the correct spectral resolution for implementing the analysis methodologies.

Regarding temporal resolution, since this project is a post-analysis of the accident, the acquisition periodicity of Sentinel-1 and Sentinel-2 images (six and five days, respectively) allows covering the study area in the days before, during, and after the spill (August 6). In a real monitoring situation of an accident with potential oil spills where mitigation measures need to be applied, these images should be complemented with other satellites/sensors. The acquisition and analysis of images with daily periodicity will allow a more detailed follow-up of the affected area.

The appropriate spatial resolution value to detect oil slicks in oceans is around 30m (Sun et al. 2016). The selected SAR (Sentinel-1) images have a spatial resolution of 5m x 20m in VV/VH polarization. The optical images from Sentinel-2 vary in spatial resolution depending on the band type. Since the analysis described here uses different bands, the 20m spatial resolution was chosen, encompassing bands 5, 7, 8, 11, and 12.

Regarding spectral resolution, Sentinel-2 multispectral images cover the necessary wavelengths for the required band compositions (Rajendran et al. 2021). All images (Table 3 for Sentinel-1 and Table 5 for Sentinel-2) were obtained for free from the Copernicus Open Access Hub website. The images were captured in the morning, which is advantageous in these regions because weather conditions are generally calmer (Rajendran et al. 2021), usually with lower wind and cloud intensity (variables that can cause noise and affect analysis results).

Different image analyses and map productions were performed using ArcGIS Pro 3.2 software with the Image Analysis extension. The Deep Learning model requires installing the respective libraries for ArcGIS, including components such as PyTorch, TensorFlow, Fast.ai, and scikit-learn (Github 2021).

### 4.1.3. Construction of Auxiliary Databases

The auxiliary database (Table 2) is an important complement in remote sensing analysis. For the geographical study area and given the proximity to the coastline, the polygon of the administrative boundaries of Mauritius Island was used as non-spectral auxiliary data. This level of information is very useful in defining land/water as well as delineating islets existing in the affected study area. Additionally, results from other studies, including delimitations of spill areas (referred to as reference slicks) published by the United Nations Satellite Centre (UNOSAT)[1] (UNOSAT 2020), were used. These data are especially useful for the thematic evaluation phase.

**Table 2**. Auxiliary database

| Layer | Source | Function |
|---|---|---|
| Administrative boundary | Esri (2023) | Delimitation of the coastline |
| Oil Spill Extent Sentinel-2 (06 Aug 2020) | UNOSAT (2020) | Support for thematic evaluation |
| Oil Spill Extent TerraSAR-X (10 Aug 2020) | UNOSAT (2020) | Support for thematic evaluation |
| Oil Spill Extent ALOS-2 (13 Aug 2020) | UNOSAT (2020) | Support for thematic evaluation |
| Oil Spill Extent TerraSAR-X (15 Aug 2020) | UNOSAT (2020) | Support for thematic evaluation |

In a more rigorous analysis, METOC data (wind direction and intensity, wave patterns, ocean currents) should be used as auxiliary data as they have a significant influence on the dispersion of the pollutant under analysis and can create noise in SAR and multispectral images (Kolokoussis & Karathanassi 2018). For this project, it was decided to exclude these variables.

### 4.1.4. Definition of Cartographic Production Strategy

The spatial analysis unit defined for this project refers to the unit where the classification algorithm is applied (Caetano 2018). As two types of data (SAR and Optical) are evaluated, the spatial analysis unit is also different. For SAR images, the classification will be based on a Deep Learning object detection method. The input raster is processed, and the result is polygons representing the object under study (probable oil slicks). For Sentinel-2 multispectral optical images, a pixel-level classification was applied. This choice was based on the homogeneity (similar spectral characteristics) of the pixels defining the oil slicks, the reduced number of classes (Land, Water, Oil, and Sediments), and the simplicity of the process. The classification result is a raster that will subsequently be converted into a vector and used in the production of the final map.

### 4.1.5. Geographical Stratification

In the geographical stratification phase, the study area is divided into subareas (strata), and each subarea is then processed separately (Caetano 2018). In this project, no stratification was performed as there are no distinct regions; the entire study area is relatively homogeneous, with no distinguishing natural or social characteristics. During the sampling stage, this decision will be considered, and samples will be created randomly within the study area.

[1] The United Nations Satellite Center (UNOSAT) is part of the United Nations Institute for Training and Research (UNITAR), with a mandate to provide United Nations funds, programs and specialized agencies with satellite analysis, training and capacity development, as well as supporting Member States in the analysis of satellite images in their respective territories and providing training and capacity development in the use of geospatial information technologies, based on voluntary contributions (UN Satellite Centre, n.d.).

## 4.2. Detection of Oil Spills with SAR Images - Sentinel-1

To identify oil spills in Sentinel-1 images, a pre-trained model "Oil Spill Detection (SAR - Synthetic Aperture Radar)" developed by ESRI was used. The various procedures from SAR data pre-processing to the application of the Deep Learning model and result evaluation are described below.

### 4.2.1. Exploratory Image Analysis

Exploratory Image Analysis is a fundamental step in image processing and data analysis, especially in remote sensing applications such as oil spill detection (Caetano 2018). As mentioned earlier, several satellite images were downloaded for different days, specifically before (29/07/2020) and during the oil spill (10/08/2020 and 16/08/2020) to evaluate its evolution (Table 3). The choice of dates was conditioned by the available images and their visibility in the area where the spill occurred.

**Table 3**. Identification of downloaded images for analysis development

| ID | Day | File Name |
|---|---|---|
| 1 | 29/07/2020 | S1B_IW_GRDH_1SDV_20200729T013754_20200729T013819_022679_02B0C2_1557_COG.SAFE |
| 2 | 10/08/2020 | S1B_IW_GRDH_1SDV_20200810T013755_20200810T013820_022854_02B625_672D.SAFE |
| 3 | 10/08/2020 | S1B_IW_GRDH_1SDV_20200810T013755_20200810T013820_022854_02B625_EF8D_COG.SAFE |
| 4 | 16/08/2020 | S1B_IW_GRDH_1SDV_20200816T143630_20200816T143704_022949_02B902_A6DD_COG.SAFE |
| 5 | 16/08/2020 | S1A_IW_GRDH_1SDV_20200816T013859_20200816T013932_033925_03EF79_F363_COG.SAFE |
| 6 | 16/08/2020 | S1A_IW_GRDH_1SDV_20200816T013859_20200816T013932_033925_03EF79_A0AD.SAFE |

Different files were considered for the three dates: one image for July 29, 2020, two different images for August 10, 2020, and three for August 16, 2020. This was considered relevant to test this model with different images and sometimes with different characteristics (pre-processing levels) such as in the case of clouds to ensure that oil spills can be identified. The images with IDs 1 to 4 were captured by the Sentinel-1B sensor, and IDs 5 and 6 by Sentinel-1A. All images were acquired in Interferometric Wide swath (IW) mode, meaning wide geographic coverage and high resolution. These images were processed to correct geometric distortions as the product type is Ground Range Detected High resolution (GRDH). Regarding polarization, all images have single polarization (1SDV).

### 4.2.2. Deep Learning Model

This subchapter describes the steps and tools used to identify oil spills in ArcGIS Pro using the Deep Learning model described in Chapter 3.

1. Despeckle: Used to correct the SAR input data for speckles resulting from coherent illumination. This tool filters out noise while retaining sharp edges and features in the SAR image (Figure 3).

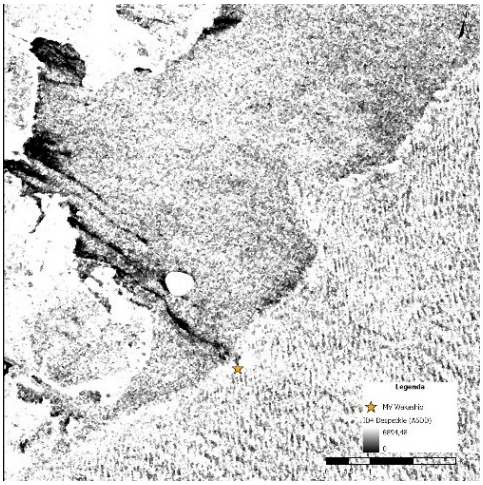


**Figure 3**. Despeckle

2. Log10: Used to convert the data scale, helping to normalize data brightness variation to make subtle differences more visible for analysis (Figure 4).

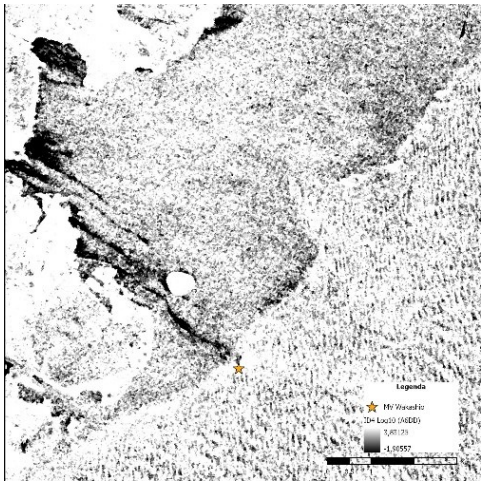


**Figure 4.** Log10

3. Clip: Used to isolate specific areas of interest, namely removing land areas that are not relevant to oil spill analysis. For this step, the Blue Bay - Pointe d'Esny (AOI) area was chosen (Figure 5).

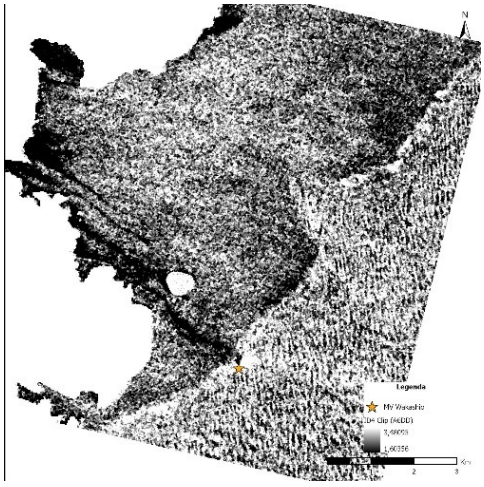


**Figure 5**. Clip

4. Composite Band: Creates a composite image from the raster with a single band (clip result) that better highlights less visible aspects and prepares the image for subsequent processing (Figure 6).

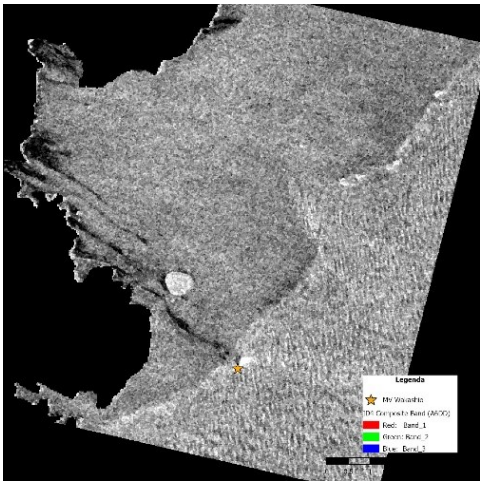


**Figure 6**. Composite Band

5. Detect Objects Using Deep Learning: Application of the pre-trained "Oil Spill Detection (SAR)" deep learning model to detect oil spills in the chosen satellite images (Figure 7).


**Figure 7**. Detect Objects Using Deep Learning

6. Pairwise Dissolve: Allows aggregating and unifying polygons based on shared attributes or geographic proximity, reducing data complexity and simplifying visualization and analysis (Figure 8).


**Figure 8**. Pairwise Dissolve

The figures presented (Figure 3 to Figure 8) demonstrate each of the steps described.

Although the spill started on August 6, 2020, the analysis of the July 19, 2020 image revealed the presence of a slick (Figure 9) which, after a more detailed visual examination, is considered a false positive that can be attributed to shallow bay areas where accumulated sediments could visually mimic an oil spill. This observation illustrates well how natural characteristics can confuse detection algorithms, particularly in shallow areas.


**Figure 9**. ID1 image analysis result

Processed images from August 10, 2020 (Figure 10 and Figure 11) show a reasonable match with the reference spill slick (auxiliary data – Table 2) indicating effective detection in coastal areas where the spill is known to have occurred (in-situ observations). However, significant slicks were also identified outside known spill areas, representing false positives that highlight the model's limitations in differentiating between spill areas and other natural or anthropogenic formations. METOC variables such as wind, ocean currents, or even elements like sediments in the water can influence SAR image analysis results (Blondeau-Patissier et al. 2023).

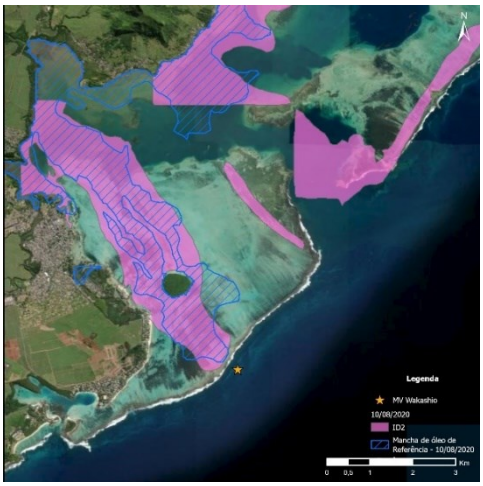


**Figure 10**. ID2 image analysis result

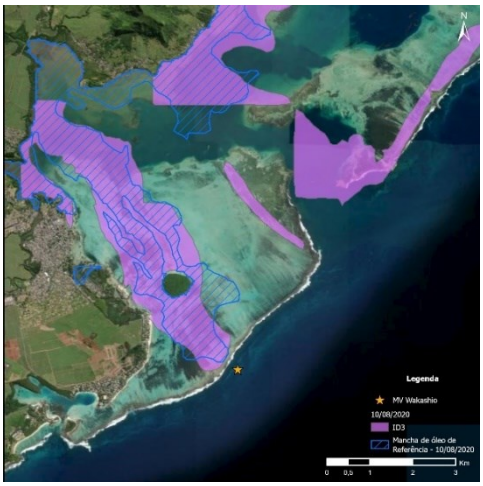


**Figure 11**. ID3 image analysis result

The analysis for August 16, 2020, shows a notable variation in model performance among the different images. In ID 4 (Figure 12) oil detection is more dispersed, identifying multiple small oil areas, indicating a fragmented model response to sea surface conditions. ID 5 (Figure 13) shows more extensive oil detection covering a large area visually aligned with the

reference slick, although it also includes areas beyond this, representing false positives. Finally, ID 6 (Figure 14) stands out by identifying two main areas; a smaller one to the south that does not correspond to the spill reference, hence considered a false positive, and a larger and more defined one along the coast indicative of oil presence. It is important to note that none of the images were able to identify the central corridor of the reference slick, and the oil spill results were more concentrated in the coastal zone, including several false positives.

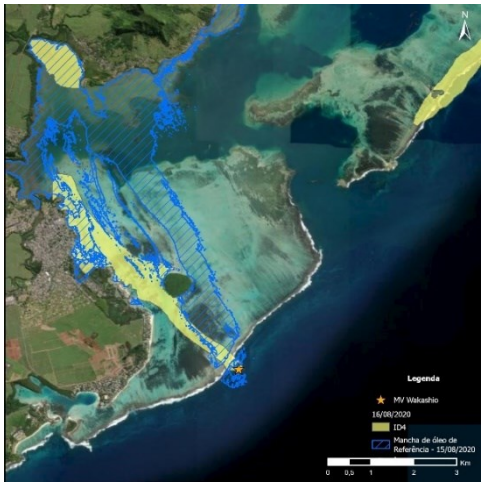


**Figure 12**. ID4 image analysis result


**Figure 13**. ID5 image analysis result


**Figure 14**. ID6 image analysis result

### 4.2.3. Thematic Accuracy Evaluation

To evaluate the accuracy of the results, it was necessary to use reference data from oil spills to compare with the model results. In this sense, the potential oil slicks identified by the UN Satellite Centre for August 10, 2020 (UNOSAT 2020a), and August 16, 2020 (UNOSAT 2020b) were used as references. The steps for this evaluation are described below:

1. Applying the defined values in the nomenclature, the study area's classification was done by assigning the value 2 to the water element and 3 to the oil element according to the reference slicks. This step resulted in three files (Figure 15):
    - For July 29, 2020, when there was no spill record yet;
    - For August 10, 2020, used to compare with the model results for the same day;
    - For August 15, 2020, used to compare with the model results for August 16, 2020;

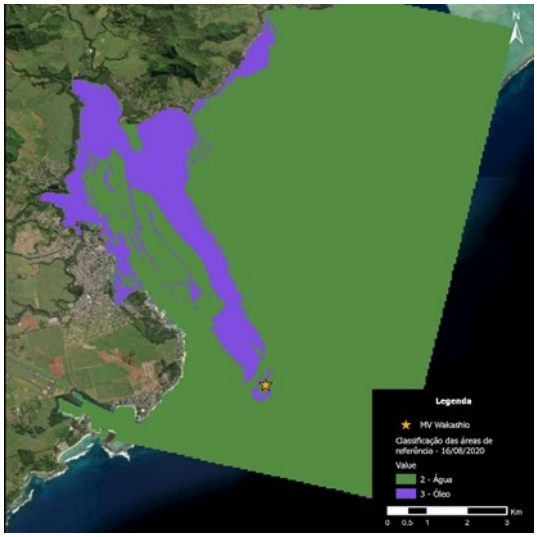


**Figure 15**. Classification of reference areas - 08/16/2020

2. Transformation of the polygons related to the reference slicks classified in the previous step into raster to serve as a basis for comparing the model results with the reference data. – This step resulted in 3 different rasters for each analysis period;
3. Create Random Points: This tool was used to create 200 reference points within the AOI (Figure 16).

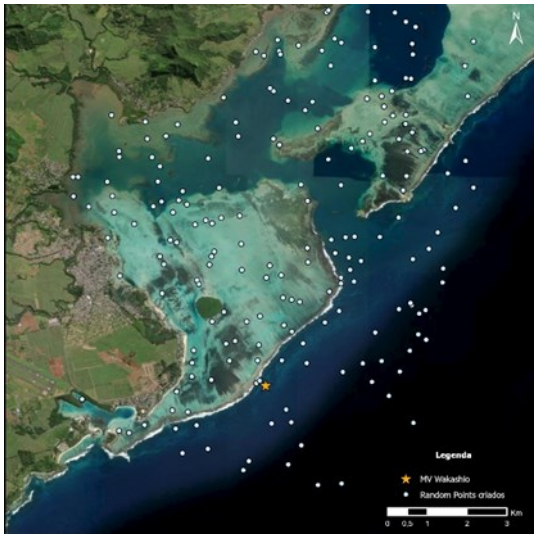


**Figure 16**. Creation of Random Points

4. Classification of the created points according to the applied pre-trained model results – This step resulted in 6 different classifications corresponding to the pre-trained model results applied to each satellite image;
5. Extract Values to Points: This tool allowed crossing the values of the points created earlier with the values assigned in the reference rasters (with reference data for each of the 3 analysis periods);
6. Exporting the result to .csv files;
7. In an Excel environment, creating confusion matrices and evaluating the model accuracy for each of the pre-trained model results (Figure 17**Error! Reference source not found.**).

ID 1 29/07/2020

| OA | 98,0 | Modelo | | | |
|---|---|---|---|---|---|
| | | 2 | 3 | Total | **UA** |
| Referência | 2 | 196 | 4 | 200 | 98,0 |
| | Total | 196 | 4 | 200 | |
| | **PA** | 100,0 | 100,0 | | |

ID2 10/08/2020 (672D)

| OA | 84,0 | Modelo | | | |
|---|---|---|---|---|---|
| | | 2 | 3 | Total | **UA** |
| Referência | 2 | 149 | 25 | 174 | 85,6 |
| | 3 | 7 | 19 | 26 | 73,1 |
| | Total | 156 | 44 | 200 | |
| | **PA** | 95,5 | 43,2 | | |

ID3 10/08/2020 (EF8D)

| OA | 85,00 | Modelo | | | |
|---|---|---|---|---|---|
| | | 2 | 3 | Total | **UA** |
| Referência | 2 | 150 | 24 | 174 | 86,2 |
| | 3 | 6 | 20 | 26 | 76,9 |
| | Total | 156 | 44 | 200 | |
| | **PA** | 96,2 | 45,5 | | |

ID4 16/08/2020 (F363)

| OA | 85,5 | Modelo | | | |
|---|---|---|---|---|---|
| | | 2 | 3 | Total | **UA** |
| Referência | 2 | 158 | 8 | 166 | 95,2 |
| | 3 | 21 | 13 | 34 | 38,2 |
| | Total | 179 | 21 | 200 | |
| | **PA** | 88,3 | 61,9 | | |

ID5 16/08/2020(A6DD)

| OA | 82,5 | Modelo | | | |
|---|---|---|---|---|---|
| | | 2 | 3 | Total | **UA** |
| Referência | 2 | 162 | 4 | 166 | 97,6 |
| | 3 | 31 | 3 | 34 | 8,8 |
| | Total | 193 | 7 | 200 | |
| | **PA** | 83,9 | 42,9 | | |

**Figure 17**. Confusion matrices of results

The confusion matrices (Figure 17) were developed as mentioned earlier in chapter 3 and allowed evaluating the results. The overall accuracy (OA) evaluation of the model indicates a generally robust

performance with accuracy rates always above 80%. However, significant variations in UA and PA for oil spill detection were observed, a crucial aspect of model performance.

On July 29, 2020, although no spill was expected, the model indicated oil detection. This result suggests a possible tendency of the model towards high sensitivity or a propensity to generate false positives, highlighting an area for improvement in model specificity and calibration.

On August 10, 2020, the model's performance in oil detection was variable, with UA and PA oscillating between moderate to reasonable. This inconsistent behavior, especially reflected by the low PA, may indicate that the model sometimes confuses other substances with oil, highlighting the need for adjustments to improve its ability to distinguish between oil and other materials present in the marine environment. Conversely, the model's detection of water was extremely precise, with high UA and PA values reaffirming the model's effectiveness in correctly identifying water areas.

On August 16, 2020, the difficulty in accurately detecting oil was even more evident, with a significantly low UA ranging from 59% to 382% and equally reduced PA. These results point to a predominance of false positives and limitations in the model's ability to effectively identify real oil spills. Despite these challenges in oil detection, the model's performance in water identification continued to be strong, with high UA metrics and reasonable PA, underscoring the model's continued utility in maritime monitoring applications where water identification is often a requirement.

This consistent performance in water detection suggests that despite failures in identifying oil spills, the model is quite accurate and reliable in identifying water bodies, maintaining its utility in marine monitoring contexts.

**Table 4**. Pre-trained Oil Spill Detection (SAR) Model Accuracy Evaluation Statistics

| ID | Day | Oil | | Water | | OA |
|---|---|---|---|---|---|---|
| | | UA | PA | UA | PA | |
| 1 | 29/07/2020 | | 100 | 98 | 100 | 98 |
| 2 | 10/08/2020 | 73,1 | 43,2 | 85,6 | 95,5 | 84 |
| 3 | 10/08/2020 | 76,9 | 45,5 | 86,2 | 96,2 | 85,0 |
| 4 | 16/08/2020 | 8,8 | 42,9 | 97,6 | 83,9 | 82,5 |
| 5 | 16/08/2020 | 38,2 | 61,9 | 95,2 | 88,3 | 85,5 |
| 6 | 16/08/2020 | 5,9 | 22,2 | 95,8 | 83,2 | 80,5 |

UA: *User's Accuracy* PA: *Producer's Accuracy* AO: *Overall Accuracy*

From the presented results, it is possible to identify that the best image for August 10, 2020, is ID3 (Figure 11) and for August 15, 2020, ID5 (Figure 13).

## 4.3. Detection of Oil Spills with Optical Images - Sentinel-2

### 4.3.1. Exploratory Image Analysis

This initial phase is fundamental for obtaining a preliminary understanding of the study area in light of the available images, identifying patterns, anomalies, and key characteristics that may affect subsequent processing and detailed analysis stages.

This study demonstrated the application of image processing techniques on multispectral optical images from the Sentinel-2 sensor for detecting an oil spill. Like SAR images, these images were obtained from the Copernicus Open Access Data website with the following characteristics (Table 5).

**Table 5.** Identification of downloaded images for analysis development

| ID | Day | File name |
|---|---|---|
| 1 | 17/07/2020 | S2B_MSIL2A_20200717T062449_N0500_R091_T40KEC_20230414T094728.SAFE |
| 2 | 06/08/2020 | S2B_MSIL2A_20200806T062449_N0500_R091_T40KEC_20230407T081024.SAFE |
| 3 | 11/08/2020 | S2A_MSIL2A_20200811T062451_N0214_R091_T40KEC_20200811T100048.SAFE |

High spatial resolution multispectral bands from Sentinel-2 were used to effectively identify oil spills with appropriate combinations of these bands to capture essential details of the spectral behavior of the elements under analysis (Rajendran et al. 2022). The images with true-color composite (RGB 432) or natural color pattern for the different dates already highlight the elements to be analyzed, as can be seen in the visual analysis of Figure 18.

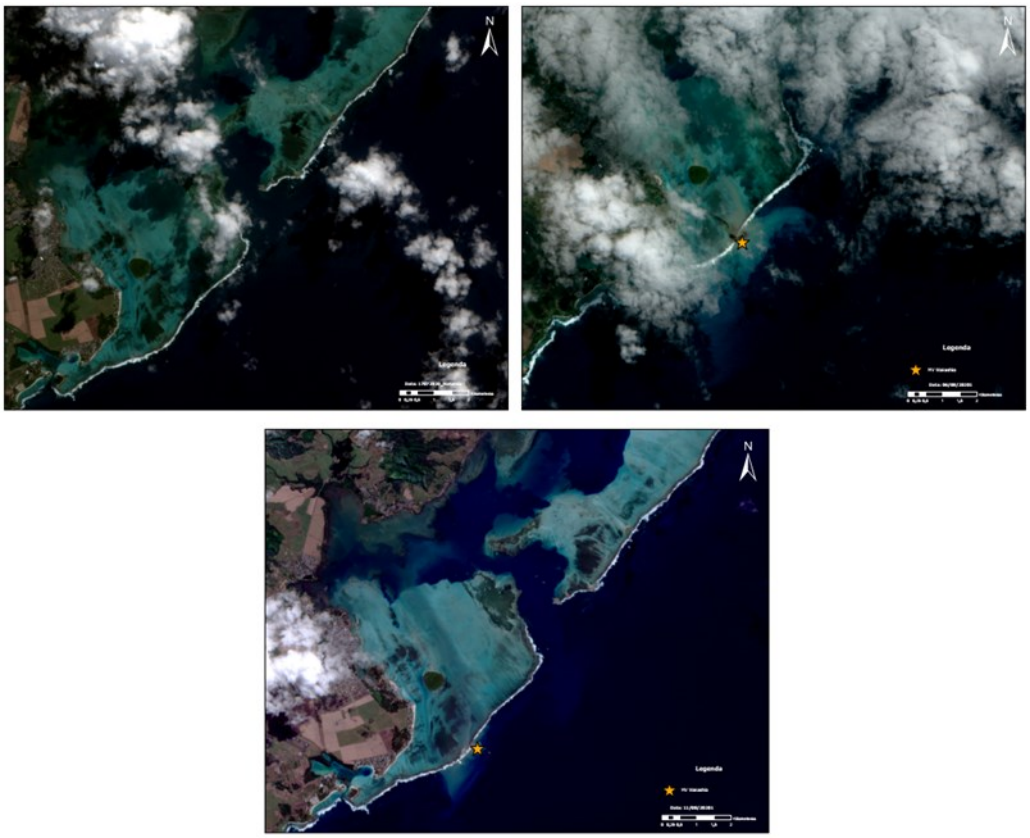

**Figure 18**. Images with "true color" color composition of the study area on the dates of 17/07/2020 (ID1), 06/08/2020 (ID2) and 11/08/2020 (ID3) respectively

In Figure 18, the image from July 17, 2020, shows no presence of the MV Wakashio ship. On this date, both the sea and the coral zone appear free of contamination, marked by the absence of any sign of oil spill or other pollutants.

Figure 19 presents the same images with the oil slick (red) and sediments (green) delimited, which show a different hue from the water.

On August 6, 2020, it was observed that the MV Wakashio ship was already stranded, evidenced in the image by the darker oil spill.

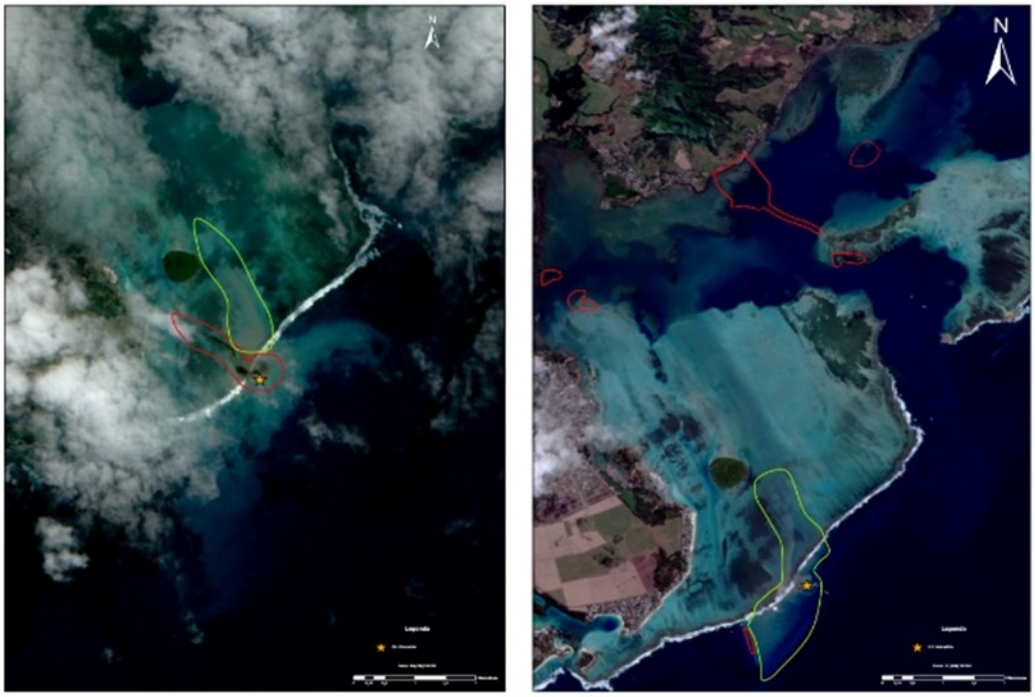

**Figure 19**. True color images with visual identification of the oil slick and sediments for the dates of 06/08/2020 and 11/08/2020 respectively

Additionally, a brownish slick indicative of sediment movement in the affected area can be noted. Subsequently, in the image from August 11, 2020, the oil spill is more dispersed, suggesting a spread of contamination over time, indicating a severe environmental situation requiring continuous monitoring. It is important to note that the image from August 6 has a high percentage of clouds. This element influences the classification results as described below. Well-defined duration events like an oil spill condition the selection of images. Working only with Sentinel-2 optical images, it was imperative to use images even with cloud presence.

### 4.3.2. Pre-Processing

In the initial phase of our study, it is essential to make specific adjustments to the image data to ensure data quality and accuracy before analysis. The pre-processing aims to correct distortions and inconsistencies in the images to improve accuracy in analysis. These steps include:

- Geometric Correction: Adjusting the image to correct perspective or tilt distortions. However, for this study, geometric corrections were unnecessary as Sentinel-2 images are pre-corrected geometrically, ensuring proper alignment and accuracy from the start.
- Radiometric Correction: Adjusting the sensor response for illumination inconsistencies, shadows, and reflections. Similarly, Sentinel-2 images also include radiometric corrections, facilitating data handling without additional adjustment steps.
- Raster Clipping: Cropping the raster image by a desired boundary. The clip raster was used to define the study area, focusing the analysis on a specific Sentinel-2 image zone. This step is important to reduce processing time and focus on the area of interest, maximizing the relevance and accuracy of the analyzed data.
- Cloud Removal: Using masks or filters to eliminate interference caused by cloud cover. In this study, cloud removal pre-processing was not performed because, according to bibliographic references (Kolokoussis & Karathanassi 2018), the authors stated that oil and oil/water

mixtures have distinct absorption characteristics from water and clouds. Thus, at this stage, the initial rasters were clipped by the study area using the clip raster tool.

### 4.3.3. Band Transformation

Sentinel-2 images are effectively used in oil spill analysis by using different band transformation combinations. This technique is fundamental for enhancing the spectral differences between bands, minimizing topographic effects (not relevant in this case as the oil spill is on the flat water surface), and facilitating the identification of specific characteristics like oil spills. Calculating new bands through band transformation significantly improves data interpretation compared to the originals, supporting the detection and analysis of oil spill extent. To explore and visualize these features, visualization tools that allow analyzing images in various spectral bands and their combinations were used. Both true-color and false-color compositions are useful for highlighting features not visible to the human eye.

The following steps were performed to create each composition (OSI and RGB) needed for subsequent analyses:

- Using the Raster Calculator tool, formulas were applied to create the necessary bands.
- Then, for the RGB composition, the three created bands were joined using the Composite Bands tool.

One of the specific spectral indices for detecting oil spills, leveraging unique spectral properties associated with oil presence in water, is the Oil Spill Index (OSI), calculated by the formula:

$$\mathrm{OSI} = \frac{\mathrm{B03} + \mathrm{B04}}{B02}$$

This index was designed to identify areas where the spectral characteristics are consistent with oil spills, using the absorption and reflection of specific Sentinel-2 bands, resulting in Figure 20, for the respective analysis dates.

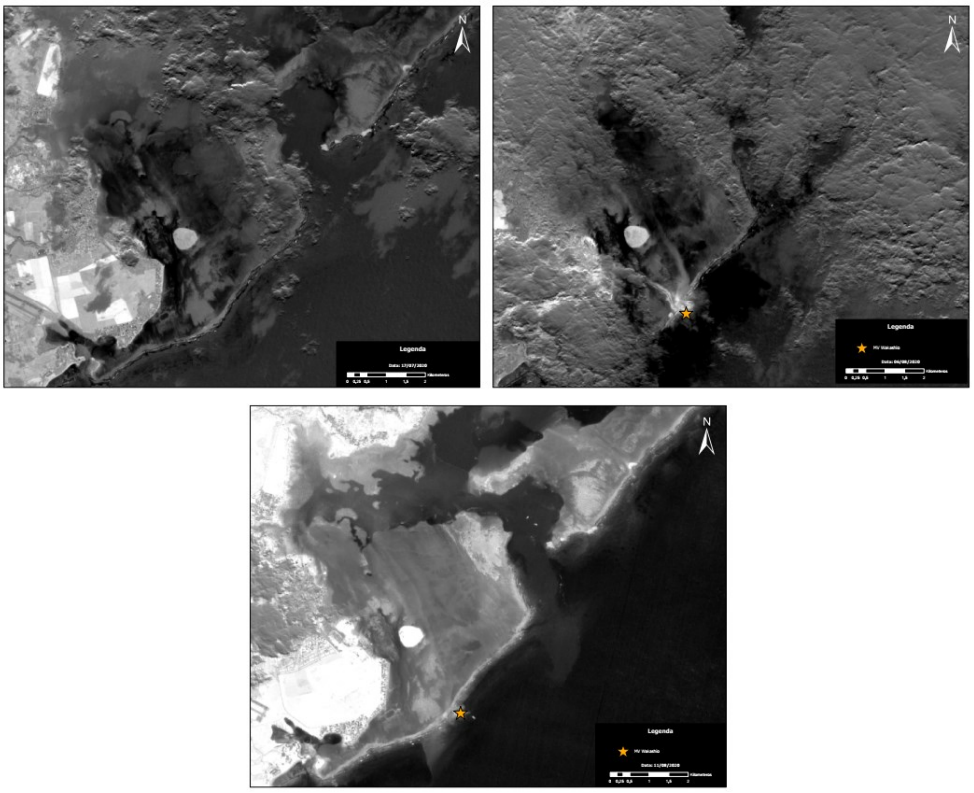

**Figure 20**. Image with application of the OSI index A. 07/17/2020, B. 08/06/2020 and C. 08/11/2020

The images in Figure 20, show the evolution of the studied area's condition with visible signs of changes in the water. The images from July 17, 2020, August 6, 2020, and August 11, 2020, transformed with the oil absorption index showed that:

- The image from July 17, 2020, displays clear water and well-defined land regions, with no significant signs of pollution or spill on this date, suggesting normal conditions in the study area.
- On August 6, 2020, there is an intensification of the dark tone in the water, indicating possible changes in the water, suggesting the presence of a spill or increased sediments.
- The last image from August 11, 2020, shows even more intense water coloration variation, with more extensive dark regions indicating the presence of the oil spill.

Another technique used is band composition, where specific combinations are formulated to maximize the contrast between water and oil, facilitating visualization and analysis. The applied composition is as follows:

- For the Red band (R): $\frac{B05+B06}{B07}$
- For the Green band (G): $\frac{B03+B04}{B02}$
- For the Blue band (B): $\frac{B11+12}{B08}$

This band combination is especially used in oil spill detection since bands 8, 8A, 11, and 12 have low reflectance of this element compared to the surrounding water (Zakzouk et al. 2024).

Band transformations are important for the practical application of environmental monitoring and disaster response management, allowing for quick and precise identification of impacted areas by oil spills, as seen in Figure 21 (Rajendran et al. 2021).

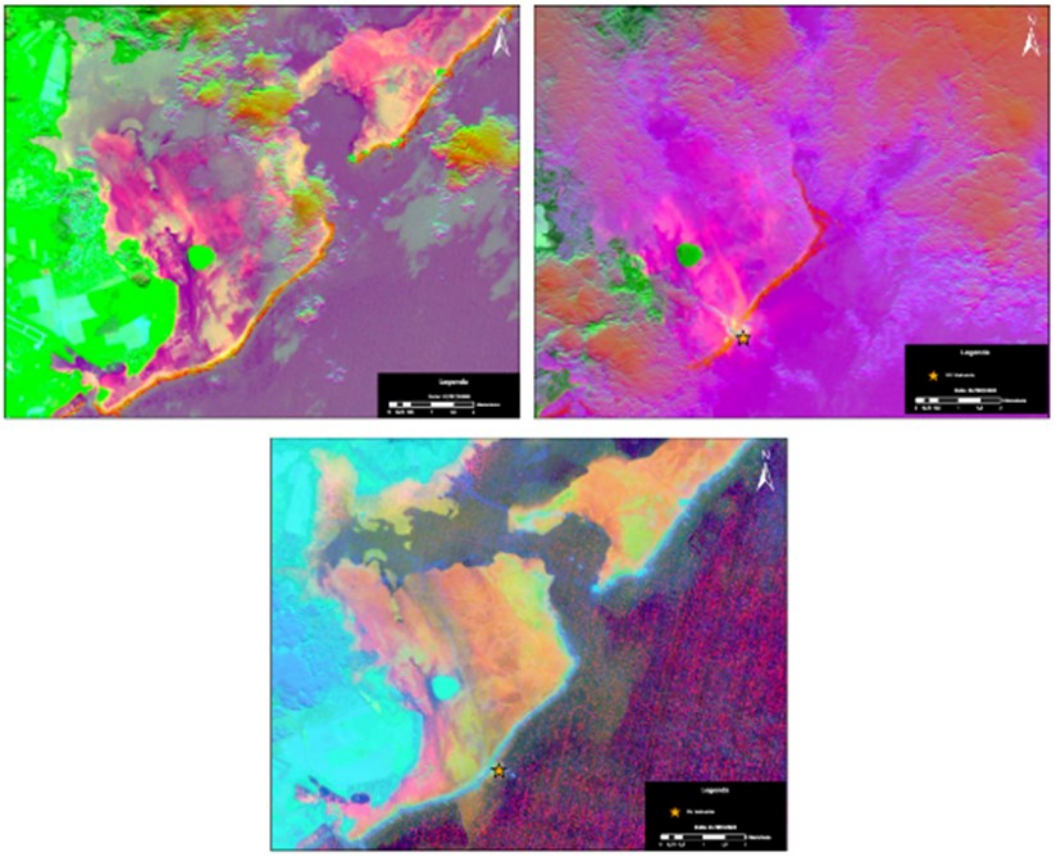

**Figure 21**. Images with composition of RGB bands - A. 07/17/2020, B. 08/06/2020 and C. 08/11/2020

In Figure 21 the results of the described composition are presented. This RGB band composition allows, through visual analysis, clear identification of various geographic and environmental features on specific dates.

- On July 17, 2020, the image shows a clear distinction between different elements. Land areas are visible in green, while water bodies are represented in shades of pink and purple. The textured brown areas highlight cloud presence, providing effective visual contrast that facilitates image interpretation. On this date, neither the ship nor oil slicks are identified in the study area.
- On August 6, 2020, significant cloud cover in brownish tones with different textures from the rest of the image indicates weather conditions that can affect the visualization of surface details. The disaster zone and ship stranding area are uncovered, so the image was kept for more detailed analysis. A yellow glow (southern zone) indicates the start of oil dispersion, a worrying sign of environmental contamination. Additionally, reddish-orange tones mark areas of shallower waters and sediment dispersion zones.
- On August 11, 2020, the oil dispersion is more extensive and visible in yellowish tones, reflecting the spill's severity on the aquatic environment. Land areas now in cyan blue confirm significant changes in spectral representation due to the progressive environmental impact and sensor response to different lighting conditions and terrain composition.

### 4.3.4. Classification

Besides the visual interpretation of images, this project includes a second approach for the supervised automatic classification of satellite images for information extraction.

In the supervised classification, the process begins by characterizing each class of the defined nomenclature based on sampling (training areas). Then, a classifier is used, which, based on the characteristics of the samples from each class, assigns a class to each pixel (Caetano 2018).

Based on the defined nomenclature for analysis, four classes were defined for classification: Land, Water, Oil, and Sediments. Thus, approximately 40 samples were created for each analyzed date to fully classify the study area.

**Supervised Classification**

In this supervised classification step, the following procedure was performed:

1. Training Phase: A theme of polygons was created to identify the classes to be represented on the map for each of the image dates, filling the attribute table “classvalue” and “classification” as specified in Table 1.
2. Then, spectral signatures were created using the Create Signatures tool.
3. After creating the spectral signatures, a dendrogram was produced using the Dendrogram tool. This process reveals the spectral similarity between the defined classes during training.
4. Finally, to elaborate the map with the predefined characteristics, the classification method was applied using the maximum likelihood algorithm with the Maximum Likelihood Classification tool.

The maximum likelihood classifier assumes that the bands have a normal distribution for each sample. With this assumption, the statistical parameters of mean and covariance are calculated for each sample. With these parameters, it is possible to calculate the probability that a given spatial analysis unit belongs to each of the classes defined in the training phase (Caetano 2018).

**Dendrograms**

Samples can be evaluated through dendrograms, which allow analyzing the relationships between the different classes defined for the training phase. In this analysis, dendrograms are quite useful for

understanding how different samples or characteristics are similar and how they cluster at different levels of similarity.

The dendrograms presented in Figure 22 reflect the spectral similarity analysis between different classes for the specific dates: July 17, 2020, August 6, 2020, and August 11, 2020.

For July 17, 2020, the classes Land and Water show relatively low spectral distance, indicating higher similarity or lower spectral distinction.

On August 6, 2020, Land and Water still show similarity, but Oil, represented as class 3, suggests clearer distinctions between the other two classes.

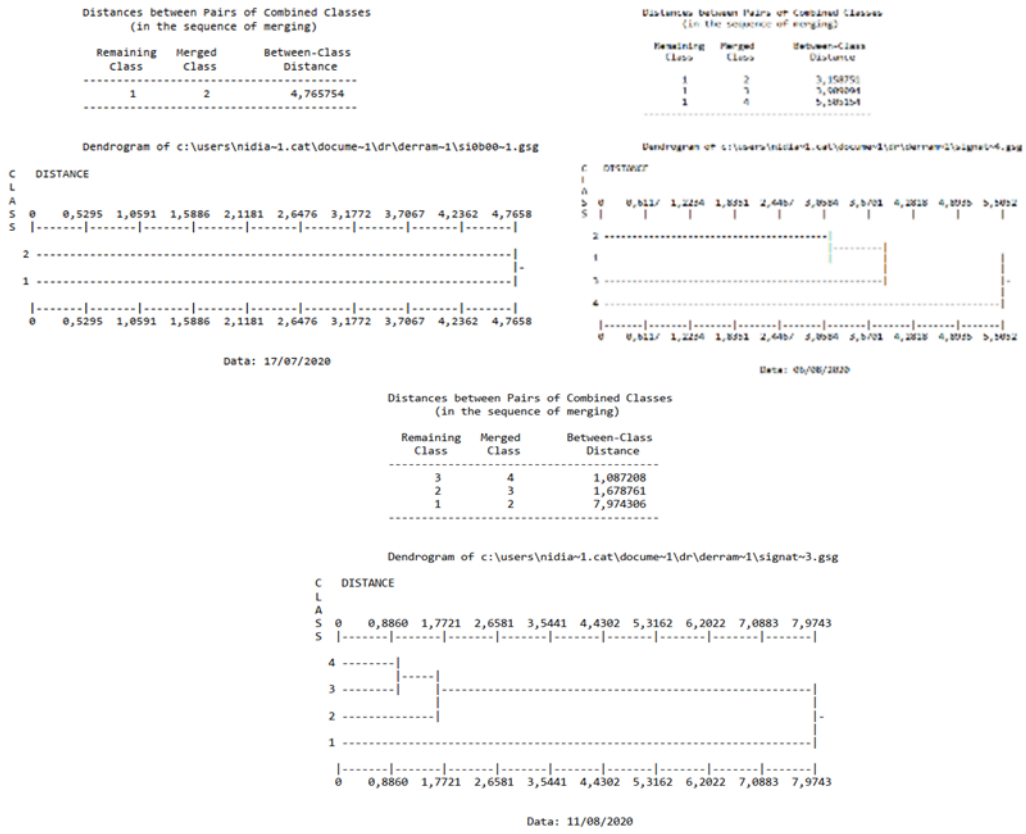


**Figure 22**. Dendrograms for the dates of 07/17/2020, 08/06/2020 and 07/11/2020 respectively

On August 11, 2020, Oil and Sediments, classes 3 and 4, respectively, initially show significant spectral distance between them, indicating well-defined distinctions between these and other classes. The spectral distance between Oil and other classes is also notably high, indicating better separability in the spectrum concerning Land and Water.

The dendrograms suggest that Land and Water have closer spectral characteristics on the initial dates, with Oil and Sediments presenting higher spectral distinction. Variation in spectral distances over dates may reflect the mixing of oil and sediments and their dispersion in water.

As a result of the supervised classification, an output raster is obtained where pixels can take values corresponding to the defined classes. Figure 23 presents the initial classification of the study area on different dates, highlighting observed changes over time.

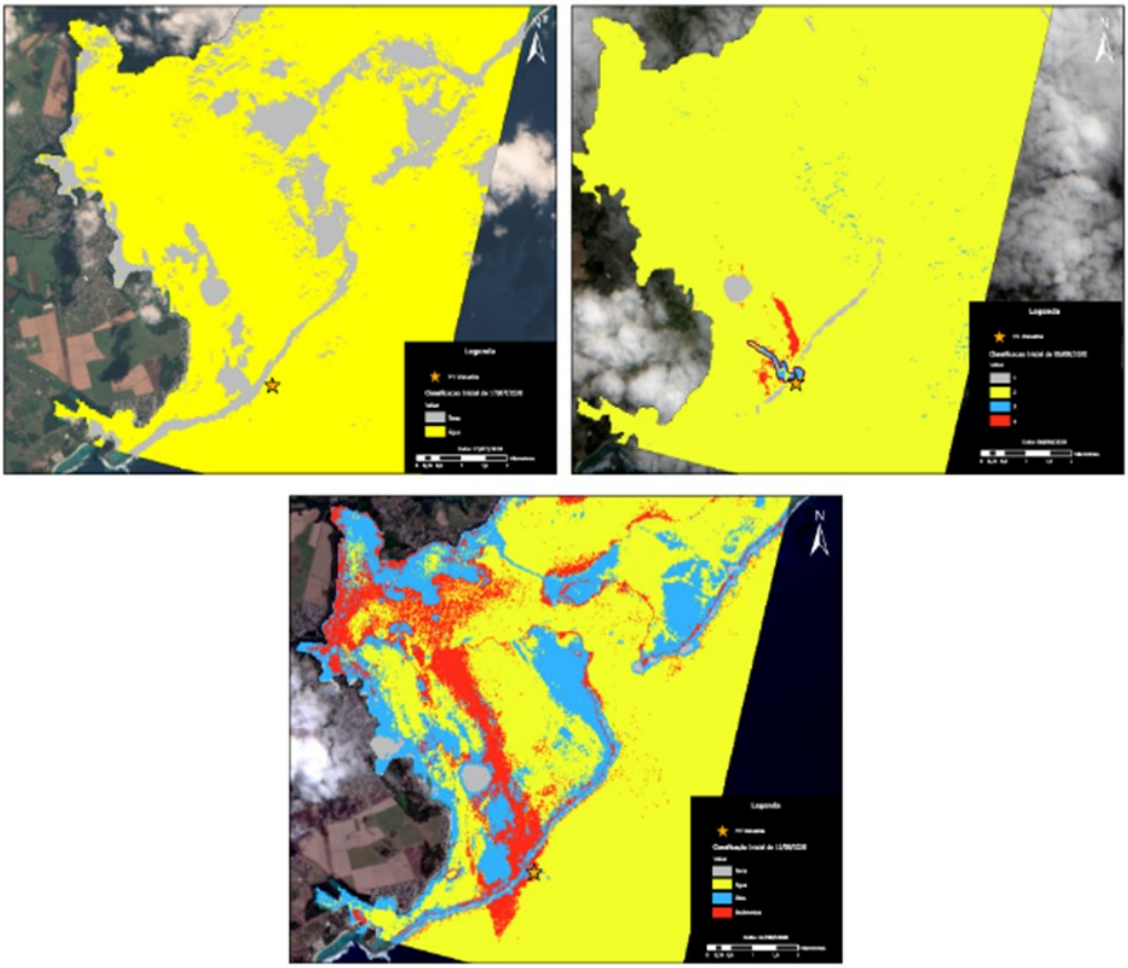

**Figure 23**. Initial Classification

On July 17, 2020, the region is free from oil contamination, reflecting a natural state before the incident.

The situation starts to change on August 6, 2020, when the first evidence of an oil spill is detected, marking the start of a significant environmental event.

On August 11, 2020, the extent of the spill is clearly visible, with a large oil slick spread across the area, indicating substantial dispersion over time.

The visual representation in the classification images reveals a salt-and-pepper effect typical of raster classifications resulting from an initial rough segmentation. This effect will be attenuated through the next post-processing step.

The analysis suggests that the classification method may need specific adjustments to better discriminate classes, especially in conditions where oil or sediments are present and mixed with other substances.

### 4.3.5. Post-Processing

The post-processing phase involved generalizing the initial classification raster and converting the raster format to vector, which was done as follows:

1. The goal of this step was to reduce the salt-and-pepper effect typical of raster classifications using the Majority Filter tool.
2. Then, the raster was converted to a vector theme using the Raster to Polygon tool.
3. Finally, to reduce the noise of the vector theme, all elements with an area less than 250 m² were selected, simplifying the map.

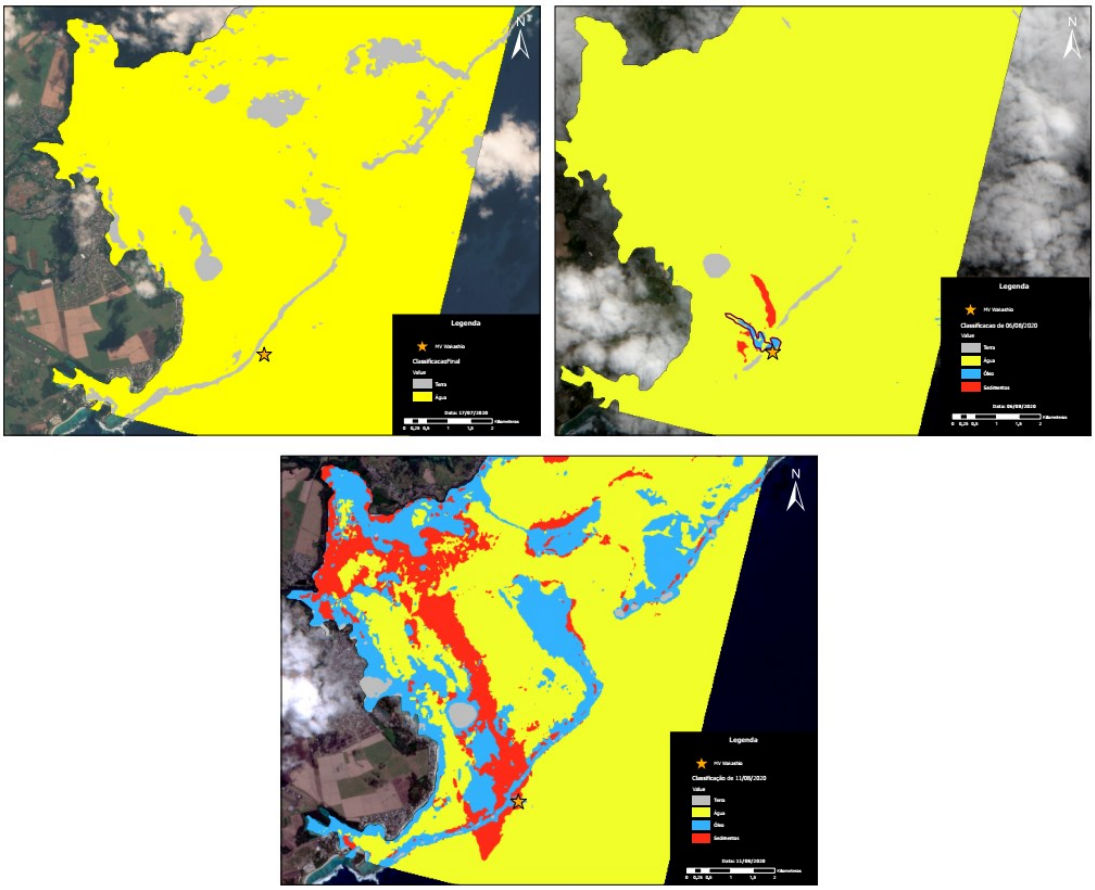

**Figure 24**. Final classification for dates: A- 07/17/2020, B- 08/06/2020, C- 08/11/2020.

After generalization and polygon creation, the following images were obtained:

1. Figure 24 which presents the final classification of the study area on different dates, highlighting observed changes over time.
    - On July 17, 2020, the region is free from oil contamination, reflecting a natural state before the incident.
    - The situation starts to change on August 6, 2020, when the first evidence of an oil spill is detected, marking the start of a significant environmental event.
    - On August 11, 2020, the extent of the spill is clearly visible, with a large oil slick spread across the bay area, indicating substantial dispersion over time.
2. Figure 25 illustrating the dramatic evolution of the oil spill observed on two critical dates. The probable oil slicks are superimposed on satellite images with a true-color composition for August 6 and August 11, 2020.
    - On August 6, 2020, the initially identified spill covered an area of 2088 hectares, indicating the start of the environmental incident. This already significant extent suggests a substantial spill or rapid oil dispersion soon after the spill began.
    - The situation escalated quickly, as evidenced by the August 11, 2020 image, where the spill expanded to an alarming extent of about 1700 hectares (it is estimated that the affected area eventually reached 2700 hectares). This exponential increase in the affected area reflects not only the severity of the spill but also the environmental conditions that may have facilitated the rapid dispersion of the oil, such as ocean currents, winds, and the underwater topography of the region.

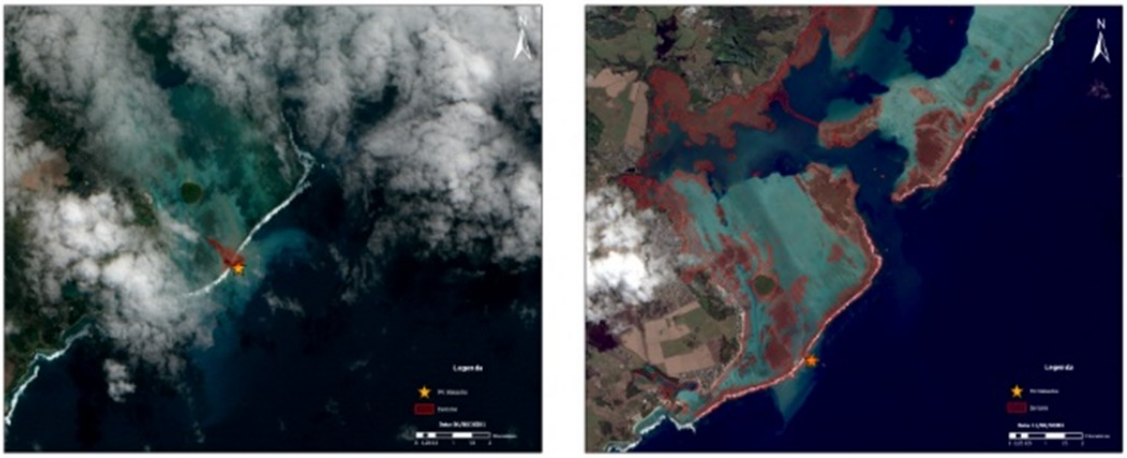

**Figure 25**. Results

### 4.3.6. Thematic Accuracy Evaluation

As described in subchapter 4.2.3 and following the same steps but changing only the number of sample points (in this case 100 were used), and based on the formulas mentioned in Chapter 3, a confusion matrix was created to evaluate the classification accuracy, calculating OA, PA, and UA for each class.

In Table 6, we can see a summary of the accuracy evaluation statistics for the three analyzed dates with Sentinel-2, understanding that the image with the best accuracy for the oil class was observed on August 6, 2020 (ID B) with a PA of 100% (UA was 50%, but the maximum PA was achieved on that date).

**Table 6**. Assisted Classification Model Accuracy Assessment Statistics (Sentinel 2)

| ID | Dia | Terra | | Água | | Óleo | | Sedimentos | | OA |
|---|---|---|---|---|---|---|---|---|---|---|
| | | UA | PA | UA | PA | UA | PA | UA | PA | |
| A | 17/07/2020 | 60 | 100 | 100 | 95 | - | - | - | - | 95 |
| B | 06/08/2020 | 25 | 33 | 97 | 97 | 100 | 50 | 100 | 100 | 94 |
| C | 11/08/2020 | 100 | 50 | 100 | 94 | 68 | 87 | 77 | 83 | 91 |

17/07/2020

| OA | 95% | Modelo | | | |
|---|---|---|---|---|---|
| | | | 2 | Total | UA |
| Referência | 1 -Terra | 3 | 5 | 8 | 60% |
| | 2 - Água | | 92 | 92 | 100% |
| | Total | 3 | 97 | 100 | |
| | PA | 100% | 95% | | |

06/08/2020

| OA | 94% | Modelo | | | | | |
|---|---|---|---|---|---|---|---|
| | | 1 | 2 | 3 | 4 | Total | UA |
| Referência | 1 -Terra | 1 | 3 | | | 4 | 25% |
| | 2 - Água | 2 | 90 | 1 | | 93 | 97% |
| | 3 - Óleo | | | 1 | | 1 | 100% |
| | 4 - Sedimentos | | | | 2 | 2 | 100% |
| | Total | 3 | 93 | 2 | 2 | 100 | |
| | PA | 33% | 97% | 50% | 100% | | |

11/08/2020

| OA | 91% | Modelo | | | | | |
|---|---|---|---|---|---|---|---|
| | | 1 | 2 | 3 | 4 | Total | UA |
| Referência | 1 -Terra | 1 | | | | 1 | 100% |
| | 2 - Água | | 67 | | | 67 | 100% |
| | 3 - Óleo | 1 | 3 | 13 | 2 | 19 | 68% |
| | 4 - Sedimentos | | 1 | 2 | 10 | 13 | 77% |
| | Total | 2 | 71 | 15 | 12 | 100 | |
| | PA | 50% | 94% | 87% | 83% | | |

**Figure 26**. Confusion Matrix

The OA evaluation of the model reveals a generally robust performance with accuracy rates above 90% on all analyzed dates (Table 6 and Figure 26).

On July 17, 2020, as expected, no oil spill was detected.

On August 6, 2020, the model's performance in oil detection was variable, with UA and PA oscillating between moderate to reasonable values. This inconsistent behavior, especially reflected by the low PA, may indicate that the model occasionally confuses other substances with oil, emphasizing the need for adjustments to improve its ability to distinguish oil from other materials present in the marine environment.

By August 11, 2020, the difficulty in accurately detecting oil was even more evident, with a considerably varying UA and relatively low PA. These results highlight the predominance of false positives and limitations in the model's ability to effectively identify real oil spills.

### 4.3.7. Validation

The accuracy of the analyses performed with Sentinel-2 is often validated through field studies where the results of image classification methods are compared with real observations. This is crucial to confirm the reliability of oil spill detection methods.

In this project, to evaluate the quality of the produced data, information provided by UNOSAT (2020) and images collected from the media (Figure 27) were used, allowing the identification of oil spills in studies over different time periods.

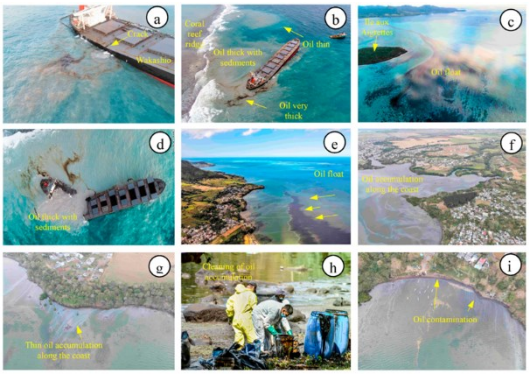


**Figure 27**. Images collected from the media (Rajendran et al., 2022)

## 4.4. Critical Comparison

The two methodological approaches/technologies for oil spill detection present advantages and disadvantages as shown in Table 7

**Table 7**. SAR and Multispectral Advantages and Disadvantages

| Sensor | SAR | Multispectral |
|---|---|---|
| Advantages | Not dependent on natural light (works day or night) or cloud presence. The contrast between oil and water is significant due to the roughness difference between the two elements. | Direct visual interpretation or band combination allowing distinction between different substances. High spatial resolution allowing detection of small-sized slicks. |
| Disadvantages | Affected by wind, ocean currents, soil moisture. | Depends on natural light (only works during the day) and clouds can obstruct the signal. |

Considering the above table, these technologies should be used complementarily for oil spill detection. SAR images can detect slicks under any weather conditions or time of day but may provide false positives, especially in "open sea" conditions with waves and current effects. In this study, false positives may also have originated from shallow water areas with sediments.

On the other hand, multispectral images can better distinguish between different types of substances, and using very high spatial resolution images can detect small oil slicks. However, they depend on natural light and favorable atmospheric conditions. When conditions allow, the combined use will be ideal, where SAR images perform the initial monitoring and multispectral images validate and follow the spill's evolution.

In maritime accidents with oil spills, obtaining images is urgent, and waiting for ideal atmospheric conditions is not possible. Thus, in cases of intense cloud cover, SAR images will be the most expedient option for an initial situation assessment.

# 5. Conclusions

In this study, the first indications of the oil spill were detected on August 6, 2020, in the Pointe d'Esny region, southeast coast of Mauritius Island, where the MV Wakashio ship ran aground using Sentinel-2 multispectral data. This spill was confirmed, and its extent evaluated through Sentinel-1 and Sentinel-2 images acquired before, during, and after the incident. The results from both sensors proved complementary and very useful in delineating the spread and accumulation of oil in the study area.

SAR images showed the MV Wakashio ship as a bright object outside the coral bay and the oil spill as dark slicks. Results from the two methodologies showed images that also displayed the accumulation of spilled oil along the coast. Over the days, the oil slicks spread in the inner bay, reaching their maximum extent on August 16, 2020, with no significant spills occurring around the ship and offshore.

Given the weather conditions (high cloud cover) in the initial days of the disaster, the SAR C-band penetrated the clouds and detected the oil spill better compared to multispectral image results.

All results were validated using aerial data and field photographs taken during the incident (available from various news channels and scientific articles).

Object detection through Deep Learning tools with a pre-trained model showed poorer thematic evaluation results than supervised classification. Even while evaluating results from two different sources (Sentinel-1 and 2), it is considered that the pre-trained model could be improved to optimize results in coastal accident cases (shallow waters and higher sediment accumulation), detect oils of different types, and recognize oil slicks of different thicknesses.

Landsat data should also be considered for this type of analysis as these multispectral images offer different spectral resolutions and bands, enriching the results when juxtaposed with Sentinel-2 data. A combined analysis integrating Landsat 8 data with Sentinel-1 and 2 could provide more comprehensive temporal and spectral coverage, potentially increasing the efficiency of oil spill detection systems (Zakzouk et al. 2024).

The ability to analyze and monitor such events over time is crucial for understanding the dynamics and extent of spills and validating the accuracy and effectiveness of detection models used. This study demonstrated the application of Sentinel-1 and 2 sensors and the potential of image processing methods to monitor and assess oil spills in oceans. The results of this study can assist decision-makers in mitigating the consequences of pollution caused by an oil spill in a specific region.

# References


Blondeau-Patissier, D., Schroeder, T., Suresh, G., Li, Z., Diakogiannis, F. I., Irving, P., Witte, C., & Steven, A. D. L. (2023). Detection of marine oil-like features in Sentinel-1 SAR images by supplementary use of deep learning and empirical methods: Performance assessment for the Great Barrier Reef marine park. Marine Pollution Bulletin, 188, 114598. https://doi.org/10.1016/j.marpolbul.2023.114598

Caetano, M. (2018). Teoria de Deteção Remota. In run.unl.pt. NOVA Information Management School. Universidade NOVA de Lisboa. https://run.unl.pt/handle/10362/115617

CCRS. (2007). Remote sensing tutorials – fundamentals of remote sensing. Canadian Centre for Remote Sensing. https://natural-resources.canada.ca/sites/nrcan/files/earthsciences/pdf/resource/tutor/fundam/pdf/fundamentals_e.pdf

ESRI. (2022, November 1). Use the model—ArcGIS pretrained models | Documentation. ESRI. https://doc.arcgis.com/en/pretrained-

models/latest/imagery/using-oil-spill-detection-sar-.htm

ESRI. (2023, August 8). Oil Spill Detection (SAR). ESRI. https://hub.arcgis.com/content/4dd65af881f64236ac9bbaa407e046ba/about

Fingas, M., & Brown, C. (2014). Review of oil spill remote sensing. Marine Pollution Bulletin, 83(1), 9–23. https://doi.org/10.1016/j.marpolbul.2014.03.059

Github. (2021). Deep Learning Libraries Installers for ArcGIS. Github. https://github.com/esri/deep-learning-frameworks

International Energy Agency (2013). World Energy Outlook 2013. https://www.iea.org/

Kolokoussis, P., & Karathanassi, V. (2018). Oil Spill Detection and Mapping Using Sentinel 2 Imagery. Journal of Marine Science and Engineering, 6(1), 4. https://doi.org/10.3390/jmse6010004

Rajendran, S., Aboobacker, V. M., Seegobin, V. O., Al Khayat, J. A., Rangel-Buitrago, N., Al-Kuwari, H. A.-S., Sadooni, F. N., & Vethamony, P. (2022). History of a disaster: A baseline assessment of the Wakashio oil spill on the coast of Mauritius, Indian Ocean. Marine Pollution Bulletin, 175, 113330. https://doi.org/10.1016/j.marpolbul.2022.113330

Rajendran, S., Vethamony, P., Sadooni, F. N., Al-Kuwari, H. A.-S., Al-Khayat, J. A., Seegobin, V. O., Govil, H., & Nasir, S. (2021). Detection of Wakashio oil spill off Mauritius using Sentinel-1 and 2 data: Capability of sensors, image transformation methods, and mapping. Environmental Pollution, 274, 116618. https://doi.org/10.1016/j.envpol.2021.116618

Sun, S., Hu, C., Feng, L., Swayze, G. A., Holmes, J., Graettinger, G., MacDonald, I., Garcia, O., & Leifer, I. (2016). Oil slick morphology derived from AVIRIS measurements of the Deepwater Horizon oil spill: Implications for spatial resolution requirements of remote sensors. Marine Pollution Bulletin, 103(1–2), 276–285. https://doi.org/10.1016/j.marpolbul.2015.12.003

UNOSAT. (n.d.). UN Satellite Centre | ReliefWeb. Reliefweb.int. https://reliefweb.int/organization/unosat

UNOSAT. (2020a, August 13). Satellite detected potential oil extent as of 10 August 2020 in Pointe d'Esny Reef, Republic of Mauritius. UNOSAT. https://unosat.org/products/2885

UNOSAT. (2020b, August 17). Satellite detected potential floating oil extent as of 15 August 2020 in Grand Port Bay, Republic of Mauritius. UNOSAT. https://unosat.org/products/2888

Zakzouk, M., El-Magd, I. A., Ali, E. M., Abdulaziz, A. M., Rehman, A., & Saba, T. (2024). Novel oil spill indices for sentinel-2 imagery: A case study of natural seepage in Qaruh Island, Kuwait. MethodsX, 12, 102520. https://doi.org/10.1016/j.mex.2023.102520

# Appendix 1 – Final Map

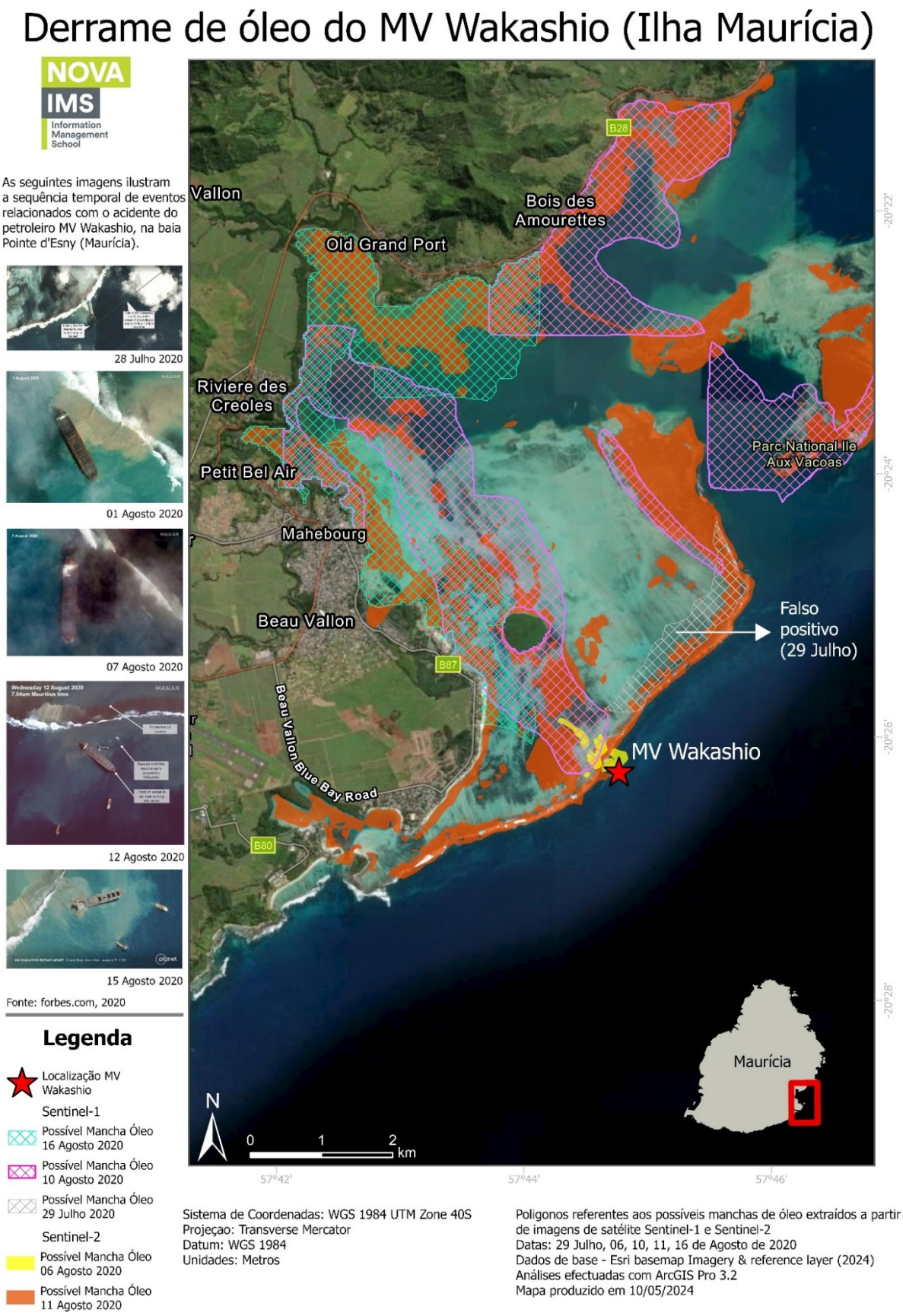


**Figure 28**. Final Map